Anomalous Topological Phases and Unpaired Dirac Cones in Photonic Floquet Topological Insulators

Daniel Leykam,[1] M. C. Rechtsman,[2] and Y. D. Chong[1,3]
[1]Division of Physics and Applied Physics, School of Physical and Mathematical Sciences, Nanyang Technological University, Singapore 637371, Singapore
[2]Department of Physics, The Pennsylvania State University, University Park, Pennsylvania 16802, USA
[3]Centre for Disruptive Photonic Technologies, Nanyang Technological University, Singapore 637371, Singapore
(Received 18 January 2016; published 29 June 2016)

We propose a class of photonic Floquet topological insulators based on staggered helical lattices and an efficient numerical method for calculating their Floquet band structure. The lattices support anomalous Floquet topological insulator phases with vanishing Chern number and tunable topological transitions. At the critical point of the topological transition, the band structure hosts a single unpaired Dirac cone, which yields a variety of unusual transport effects: a discrete analogue of conical diffraction, weak antilocalization not limited by intervalley scattering, and suppression of Anderson localization. Unlike previous designs, the effective gauge field strength can be controlled via lattice parameters such as the interhelix distance, significantly reducing radiative losses and enabling applications such as switchable topological waveguiding.

DOI: 10.1103/PhysRevLett.117.013902

Photonic topological insulators (PTIs) are an emerging class of photonic devices possessing topologically nontrivial gapped photonic band structures [1–18], analogous to single-particle electronic band structures of topological insulators [19]. They have potential applications as robust unidirectional or polarization-filtered waveguides, and as scientific platforms for probing topological effects inaccessible in condensed-matter systems. In the technologically important optical frequency regime, only two PTIs have been demonstrated in experiment: arrays of helical optical waveguides [10], and coupled ring resonators [11–13,15,17]. These two different designs each possess unique advantages. Waveguide array PTIs, for instance, allow the propagation dynamics of topological edge states to be directly imaged [10]. The design of the waveguide array PTI is based on the "Floquet topological insulator" concept [20–23], which originally described quantum systems with time-periodic Hamiltonians; the idea is that topologically nontrivial states can be induced via periodic driving [20–23], rather than via magnetic or spin-orbit effects in a static Hamiltonian. In the PTI, the Hamiltonian describes the classical evolution of the optical fields in the waveguide array, and its periodic drive arises from the helical twisting of the waveguides [10,24].

Floquet topological insulators are highly interesting because they exhibit topological phenomena that have no counterparts in static Hamiltonians [25–32]. For example, there can exist two-dimensional (2D) "anomalous Floquet insulator" (AFI) phases that are topologically nontrivial—including hosting protected edge states—despite all bands having zero Chern number [15,17,26–30]. When disorder is introduced, the anomalous topological edge states become the only extended states, with all other states localized [31]. At critical points between topological phases, Floquet band structures can exhibit unpaired Dirac cones, defeating the "fermion-doubling" principle [33]. It is thus noteworthy that these unusual features were *not* accessed by the experiments of Ref. [10]. The waveguide array was always observed in a standard Chern insulator phase generated by weak periodic driving; transitions to any other topologically nontrivial phase were unachievable because the strength of the effective gauge field was controlled by the bending radius of the helical waveguides. Radiative losses, which increase exponentially with bending [34], came to dominate before any "strong field" topological transitions were reached [10].

This paper describes a class of waveguide arrays overcoming the above limitations, allowing for the observation of topological transitions between conventional insulator, Chern insulator, and AFI phases, as well as unpaired Dirac cones at the transition points. To the best of our knowledge, AFI phases and unpaired Dirac cones have never been demonstrated in optical-frequency PTIs. Continuously tuned transitions between trivial and nontrivial topological phases, or into an AFI phase, have never been observed in any 2D PTI. Our design is based on "staggered" lattices of helical waveguides, with each of the two sublattices having a different helix phase. The two-band Floquet band structure can be tuned to different topological phases by varying the nearest-neighbor coupling strength or sublattice asymmetry. We can access different topological phases while maintaining small bending radii; the bending losses for reaching the conventional insulator to the AFI transition are reduced by around 2 orders of magnitude compared to the topological transition discussed in Ref. [10]. This design thus shows promise for low-loss topological waveguides that are switchable (e.g., via optical nonlinearity).

 © 2016 American Physical Society

The critical Floquet band structure hosts an unpaired Dirac cone. This is unlike all other previously observed photonic band-crossing points, which involve either paired Dirac points [35], quadratic dispersion [36], or an attached flat band [37,38]. The unpaired Dirac cone is reminiscent of the chiral band structure of the Haldane model with broken parity and time-reversal symmetries [39], or surface states of three-dimensional topological insulators [19,40]. Here, it arises from a Floquet process, and specifically the fact that the Floquet band structure is a "quasienergy" spectrum (see below). Wave propagation in the critical PTI is immune to the intervalley scattering that occurs with pairs of Dirac cones [41]. Based on this, we demonstrate a novel "discrete" conical diffraction effect, generated by exciting a single unit cell, as well as resistance to localization in the presence of short-range disorder [42]. We note that although similar Floquet band structures that can host unpaired Dirac cones have previously been studied theoretically [13,21,33], those studies lacked information about the propagation dynamics of the Dirac cone states, which we can investigate using our experimentally realistic waveguide array models.

An example of the staggered helix design is the square lattice shown in Figs. 1(a) and 1(b). There are two sublattices, forming a checkerboard pattern; the helices on each sublattice are shifted relative to each other in the z direction, by half a helix cycle. This produces a z-dependent separation between waveguides, so that each waveguide approaches its four nearest neighbors in turn at each quarter cycle. Similar schemes can be implemented in other lattice geometries, such as a honeycomb lattice [27]. For simplicity, this Letter focuses on the square lattice.

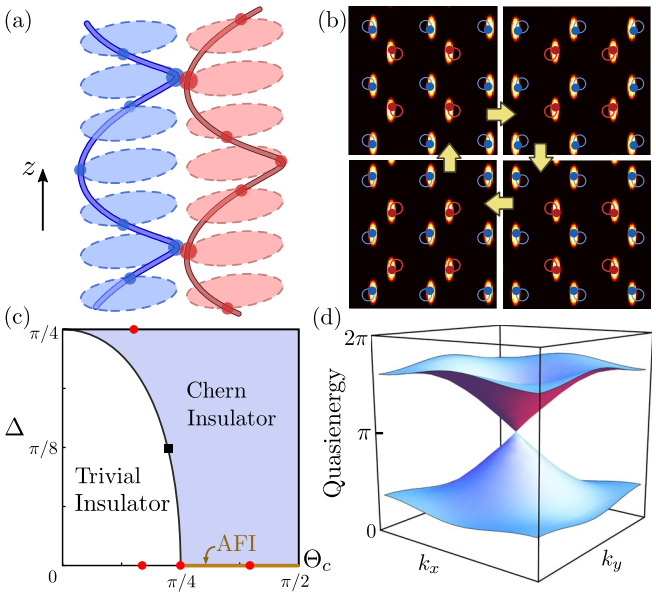

FIG. 1. A square staggered lattice of helical waveguides. (a) Schematic of two neighboring waveguides, twisting clockwise along the propagation axis z with relative phase shift π. (b) Cross section of the lattice potential at each helix quarter cycle, with the circular trajectories overlaid. (c) Phase diagram of the tight-binding model, in terms of the sublattice asymmetry Δ and coupling strength θ_c. Red dots indicate the parameters for the band diagrams in Fig. 2. The nontrivial phase forms an AFI along the $\Delta = 0$ line and a Chern insulator for $\Delta \neq 0$. (d) Tight-binding bulk spectrum at the black square in (c), along the phase boundary.

First, we model the lattice in a tight-binding approximation similar to a 2D discrete-time quantum walk [43]. Since the interwaveguide couplings are evanescent, we assume each waveguide couples to one neighbor at a time. The Floquet evolution operator, $\hat{U}$, is defined by $\psi(z+Z) = \hat{U}\psi(z)$, where Z is the helix period and $\psi = (\psi_A, \psi_B)$ are the tight-binding amplitudes on each sublattice. $\hat{U}$ factorizes into a series of independent two-waveguide couplings, separated by free evolution,

$$\hat{U} = \hat{S}(-k_-)\hat{S}(-k_+)\hat{S}(k_-)\hat{S}(k_+), \tag{1}$$

with the notation $k_\pm \equiv (k_x \pm k_y)/\sqrt{2}$, where $k_{x,y}$ are the crystal momenta in units of the inverse waveguide separation in the absence of modulation, and

$$\hat{S}(\kappa) = \begin{pmatrix} e^{i\Delta}\cos\theta_c & -ie^{i(\Delta+\kappa)}\sin\theta_c \\ -ie^{-i(\Delta+\kappa)}\sin\theta_c & e^{-i\Delta}\cos\theta_c \end{pmatrix}, \tag{2}$$

where Δ is a small detuning between the sublattice propagation constants (which can be implemented by having different waveguide refractive indices), and θ_c is the coupling strength. Since $\hat{U}$ is unitary, its eigenvalues have the form $e^{i\beta(\boldsymbol{k})}$ where $\beta(\boldsymbol{k})$ is the quasienergy spectrum. Note that this model resembles the 2D quantum walk described in Ref. [26], with time evolution replaced by propagation in z, and that $\hat{S}(\kappa)$ is the most general scattering matrix permitted by the lattice symmetries [44].

Figure 1(c) shows the phase diagram of the quasienergy band structure, as a function of Δ and θ_c. The system is a trivial insulator at weak couplings, and a topological insulator above a critical coupling strength [44]. At the transition, the band structure has an unpaired Dirac cone at the Γ point, as shown in Fig. 1(d). Increasing Δ pushes the two bands away from quasienergy $\beta = 0$ and closer towards reconnecting at $\beta = \pm\pi$, reducing the critical coupling strength. At $\theta_c = \pi/2$, the bands merge into a topological flat band [26].

The $\Delta = 0$ case is particularly interesting. Here, the sublattice symmetry enforces a line degeneracy at the Brillouin zone edge, so there is a single band gap. For small θ_c, the spectrum resembles that of an unmodulated square lattice with a single Bloch band folded back onto itself. At the critical point $\theta_c = \pi/4$, the formation of the Dirac cone leads to a completely gapless spectrum. A long-wavelength expansion of $\hat{U} \approx \exp[-i(\hat{H}_D - \pi)]$ about the Γ point yields an effective Dirac Hamiltonian,

$$\hat{H}_D(\boldsymbol{k}) = -k_x\hat{\sigma}_z + k_y\hat{\sigma}_y - 4(\theta_c - \pi/4)\hat{\sigma}_x, \qquad (3)$$

where $\hat{\sigma}_{x,y,z}$ are the Pauli matrices. For $\theta_c > \pi/4$, the system is an AFI [26–30] with unidirectional topological edge states.

To apply these ideas to a realistic photonic lattice, such as femtosecond laser-written waveguides in fused silica [10,29,45], we now go beyond the tight-binding description. A photonic lattice is described by a paraxial field $\psi(\boldsymbol{r}, z)$ governed by the Schrödinger equation

$$i\partial_z\psi = -\frac{1}{2k_0}\nabla_\perp^2\psi - \frac{k_0\delta n(x,y,z)}{n_0}\psi, \qquad (4)$$

where $\nabla_\perp^2 = \partial_x^2 + \partial_y^2$, $k_0 = 2\pi n_0/\lambda$, and the refractive index is $n_0 = 1.45$ at wavelength $\lambda = 633$ nm, with modulation $\delta n \sim 7.5 \times 10^{-4}$. Similar to real experiments, we give the waveguides elliptical cross sections with axis diameters 11 and 4 μm [10], as shown in Fig. 1(b). They form a square lattice with mean waveguide separation a, helix radius R_0, and pitch Z. We can increase the effective coupling, θ_c, by increasing $1/a$, R_0, or Z.

Direct calculation of the Floquet band structure for a continuum model (as opposed to a tight-binding model) is a nontrivial task, because the quasienergies $\beta_{n,\boldsymbol{k}}$ are defined modulo $2\pi/Z$, so there is no ground state for numerical eigensolvers to converge on, and continuum (unguided) modes enter in an uncontrolled way. We devised an efficient method for performing this calculation by truncating the evolution operator $\hat{U}$ to a basis formed by the *static* Bloch waves at $z = 0$. This amounts to a quasistatic approximation neglecting coupling to unbound (continuum) modes. Bending losses can be estimated via the norm of the Floquet evolution operator eigenvalues, by findings its deviation from unitarity. Further details are given in Supplemental Material [44].

We now fix $R_0 = 3$ μm and $Z = 2$ cm. This yields a loss of $\lesssim 0.02$ dB/cm, independent of topological phase, which we tune by varying a and/or Δ. By contrast, the strength of the effective gauge field in the unstaggered lattice of Ref. [10] was tuned by increasing R_0, which also increased the bending losses exponentially [34]. That limited the system to the "weak field" perturbative regime; losses exceeded 3 dB/cm before reaching a predicted strong field topological transition (between two Chern insulators), making that transition unobservable.

Figure 2 shows the band structure for a strip geometry. For comparison, results from the truncated-Bloch method are plotted together with the results from a fitted tight-binding model [44]. The two methods agree well, particularly in the weak-coupling regime. In Fig. 2(a), we see that the system is a trivial insulator, with a single band and a single gap (note that the spectrum is periodic along the β axis), whereas in Fig. 2(b), the gap has closed and reopened, inducing chiral edge states centered at $\beta \sim \pi$.

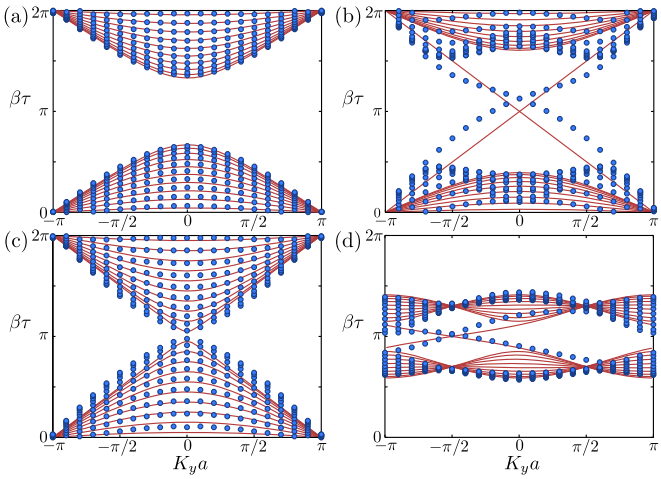

FIG. 2. Band structures for a semi-infinite strip ten unit cells wide. Blue points are obtained from the continuum model, and red curves from the tight-binding model. (a) Trivial insulator ($a = 25$ μm, $\theta_c \approx 0.17\pi$, $\Delta = 0$). (b) Anomalous Floquet insulator ($a = 20$ μm, $\theta_c \approx 0.4\pi$, $\Delta = 0$). (c) Critical phase ($a = 23$ μm, $\theta_c \approx \pi/4$, $\Delta = 0$). (d) Chern insulator ($a = 23$ μm, $\theta_c \approx 0.15\pi$, $\Delta \approx \pi/4$).

This is the AFI phase; the Chern number of the single band is necessarily 0, despite the presence of chiral edge states. The transition point is shown in Fig. 2(c), which features an unpaired Dirac point at the center of the Brillouin zone. Figure 2(d) shows a $\Delta \neq 0$ case, corresponding to a Chern insulator; there is both a trivial gap and a nontrivial gap, and the two bands have Chern numbers 1 and -1, as in the Haldane model [46].

The topological transitions can be probed via beam propagation experiments. Figure 3 shows beam propagation simulations with a single waveguide initially excited along the edge. For large a, with the lattice in the trivial phase, the excitation simply spreads into the bulk. Upon decreasing a, we observe a strongly localized mode that

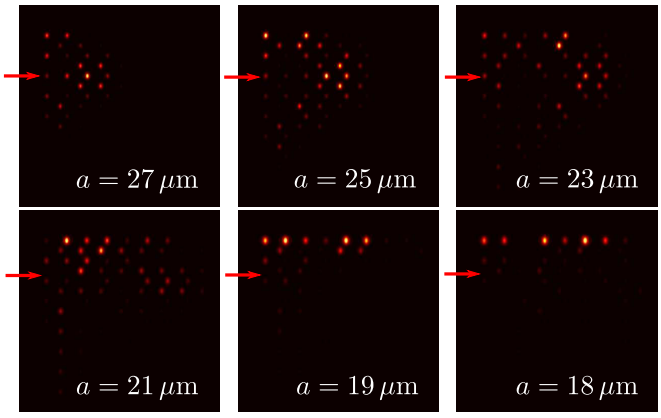

FIG. 3. Output intensity profile after propagation through $5Z$, with one edge site initially excited (red arrow). Reducing the lattice period causes a transition into an anomalous Floquet insulator phase with topological edge states.

propagates unidirectionally along the edge, including around corners. This is a clear signature of a topological transition to the AFI, which has never been experimentally demonstrated in a 2D photonic lattice. We stress that varying a is just one of many possible tuning methods. Because of the strong sensitivity of the evanescent coupling strength to waveguide mode localization, there are other interesting ways to achieve controllable switching between topological phases, such as the Kerr effect or thermal tuning.

It is also interesting to study the behavior of the lattice at the critical point of the topological transition, where the quasienergy band structure contains an unpaired Dirac cone at the Brillouin zone center. A direct method for revealing the existence of a Dirac cone is conical diffraction, which involves constructing an initial wave packet from Dirac cone states, which then evolves (under linear relativistic dispersion) into a ring with constant thickness and nonzero phase winding. In honeycomb lattices with two Dirac cones, conical diffraction requires selectively exciting one cone, e.g., using a tilted spatially structured input beam [35]. With an unpaired Dirac cone, however, we can generate conical diffraction using simple unstructured Gaussian beams at normal incidence, as shown in Figs. 4(a) and 4(b). This exclusively excites "pseudospin-up" Dirac modes governed by Eq. (3), with chirality determined by the chirality of the modulation $\delta n(\boldsymbol{r}, z)$. This intrinsic chirality is revealed by the phase of the diffracted field. Pseudospin angular momentum generates an optical vortex in the "cross-polarized" pseudospin-down component of the diffracted field, with vortex charge sensitive to the chirality of the Dirac dispersion [47]. Here, pseudospin down corresponds to light scattered into the second Brillouin zone, readily measured via Fourier filtering [44]. Figure 4(c) shows the phase profile, exhibiting the predicted topological charge.

What happens as we reduce the width of the initial Gaussian excitation? One might expect conical diffraction to be destroyed, since Eq. (3) is based on an effective-mass (carrier-envelope) approximation in the transverse plane. While that is the case for static Hamiltonians, here diffraction is preserved by the unique features of the Floquet band structure: the spectrum is entirely gapless, and has no local band maxima or minima. Consequently, the band velocity is nonzero almost everywhere, and the initial excitation evolves into a discrete conical-like diffraction pattern with a dark central spot and nonzero vortex charge. As shown in Figs. 4(d)–4(f), this holds true even when the initial excitation is reduced to a single unit cell.

Wave propagation at the critical point should be intrinsically robust against disorder, due to the enforced chirality and absence of band edges. To show this, we introduce random site-to-site fluctuations in the waveguide detunings of the tight-binding model (1). For weak disorder, Dirac modes experience suppressed backscattering, a phenomenon known as "weak antilocalization" [42]. Usually, weak antilocalization disappears when the disorder is short ranged, due to intervalley scattering [41]. However, Fig. 5(a) shows that weak antilocalization persists in our system even for completely short-range (site-specific) disorder. Furthermore, Anderson localization normally sets in at large disorder strengths, commencing at the band edges. In Fig. 5(b), we probe the localization of the tight-binding eigenmodes by their mode participation numbers, and find that localization is defeated in the critical $\Delta = 0$ system due to the lack of band edges. For $\Delta \neq 0$, the Floquet band structures have well-defined band edges, and we correspondingly observe Lifshitz tails of strongly localized modes [44].

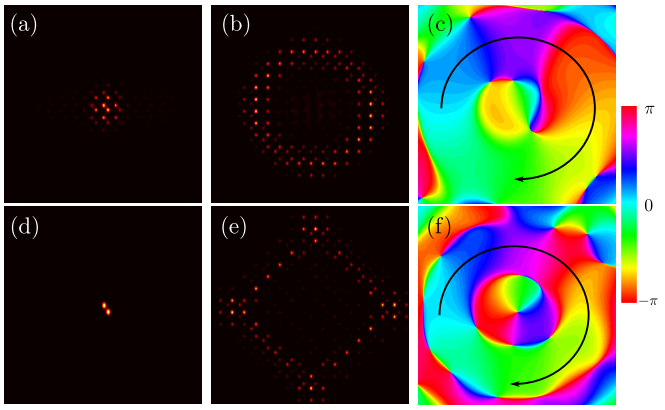

FIG. 4. Conical diffraction arising from the unpaired Dirac point. In the upper panels, the initial excitation is Gaussian; in the lower panels, only one unit cell is excited. [(a) and (d)] Input and [(b) and (e)] output beam intensity. [(c) and (f)] Phase profile of the output cross-polarized pseudospin component, showing clockwise phase circulation (black arrows). The lattice size is 16×16 unit cells, and the propagation distance is $L = 6Z$.

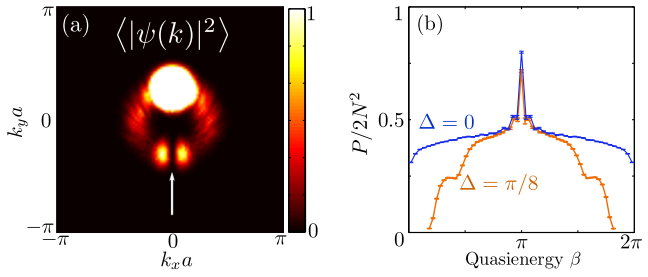

FIG. 5. Disorder insensitivity at the critical point. (a) Fourier intensity of a broad (width $5a$) probe beam, after propagating $60Z$ through a weakly disordered [44] 100×100 lattice, averaging over 20 disorder realizations. A weak antilocalization dip occurs in the backscattering direction (white arrow); the color scale saturates in the forward direction. (b) Participation number P normalized by number of waveguides $2N^2 = 1800$, for the tight-binding eigenmodes of a strongly disordered lattice. Localization is absent for $\Delta = 0$, but Lifshitz localization tails appear for $\Delta = \pi/8$.

In summary, we have shown how to realize Floquet PTIs in staggered helical waveguide arrays. Novel topological transitions, beyond those characterized by Chern numbers, can be accessed by tuning lattice parameters other than the bending radius; this allows for low-loss operation and raises the prospect of nonlinear or actively controllable, robust topological waveguide devices [48]. The many interesting behaviors of the unpaired Dirac cone at the critical point, including discrete conical diffraction and suppression of Anderson localization, are worth probing in detail in future experiments.

We are grateful to N. H. Lindner and H. Wang for helpful discussions. This research was supported by the Singapore National Research Foundation under Grant No. NRFF2012-02, and by the Singapore MOE Academic Research Fund Tier 3 Grant No. MOE2011-T3-1-005. M. C. R. acknowledges the support of the National Science Foundation under Grant No. ECCS-1509546.

[1] L. Lu, J. D. Joannopoulos, and M. Soljačić, Topological photonics, Nat. Photonics **8**, 821 (2014). Note that the term insulator indicates only that the photonic band structure is gapped; there is no notion of a Fermi level since photons are bosonic.

[2] F. D. M. Haldane and S. Raghu, Possible Realization of Directional Optical Waveguides in Photonic Crystals with Broken Time-Reversal Symmetry, Phys. Rev. Lett. **100**, 013904 (2008).

[3] S. Raghu and F. D. M. Haldane, Analogs of quantum-Hall-effect edge states in photonic crystals, Phys. Rev. A **78**, 033834 (2008).

[4] Z. Wang, Y. Chong, J. D. Joannopoulos, and M. Soljačić, Observation of unidirectional backscattering-immune topological electromagnetic states, Nature (London) **461**, 772 (2009).

[5] N. Malkova, I. Hromada, X. Wang, G. Bryantand Z. Chen, Observation of optical Shockley-like surface states in photonic superlattices, Opt. Lett. **34**, 1633 (2009).

[6] R. O. Umucalılar, and I. Carusotto, Artificial gauge field for photons in coupled cavity arrays, Phys. Rev. A **84**, 043804 (2011).

[7] K. Fang, Z. Yu, and S. Fan, Realizing effective magnetic field for photons by controlling the phase of dynamic modulation, Nat. Photonics **6**, 782 (2012).

[8] Y. E. Kraus, Y. Lahini, Z. Ringel, M. Verbin and O. Zilberberg, Topological states and adiabatic pumping in quasicrystals, Phys. Rev. Lett. **109**, 106402 (2012).

[9] A. B. Khanikaev, S. H. Mousavi, W.-K. Tse, M. Kargarian, A. H. MacDonald, and G. Shvets, Photonic topological insulators, Nat. Mater. **12**, 223 (2013).

[10] M. C. Rechtsman, J. M. Zeuner, Y. Plotnik, Y. Lumer, D. Podolsky, F. Dreisow, S. Nolte, M. Segev, and A. Szameit, Photonic Floquet topological insulators, Nature (London) **496**, 196 (2013).

[11] M. Hafezi, S. Mittal, J. Fan, A. Migdall, and J. M. Taylor, Imaging topological edge states in silicon photonics, Nat. Photonics **7**, 1001 (2013).

[12] G. Q. Liang and Y. D. Chong, Optical Resonator Analog of a Two-Dimensional Topological Insulator, Phys. Rev. Lett. **110**, 203904 (2013).

[13] M. Pasek and Y. D. Chong, Network models of photonic Floquet topological insulators, Phys. Rev. B **89**, 075113 (2014).

[14] C. He, X.-C. Sun, X.-P. Liu, M.-H. Lu, Y. Chen, L. Feng, and Y.-F. Chen, Photonic topological insulator with broken time-reversal symmetry, Proc. Natl. Acad. Sci. U.S.A. **113**, 4924 (2016).

[15] W. Hu, J. C. Pillay, K. Wu, M. Pasek, P. P. Shum, and Y. D. Chong, Measurement of a Topological Edge Invariant in a Microwave Network, Phys. Rev. X **5**, 011012 (2015).

[16] J. M. Zeuner, M. C. Rechtsman, Y. Plotnik, Y. Lumer, S. Nolte, M. S. Rudner, M. Segev, and A. Szameit, Observation of a Topological Transition in the Bulk of a non-Hermitian System, Phys. Rev. Lett. **115**, 040402 (2015).

[17] F. Gao, Z. Gao, X. Shi, Z. Yang, X. Lin, J. D. Joannopoulos, M. Soljačić, H. Chen, L. Lu, Y. Chong, and B. Zhang, Probing the limits of topological protection in a designer surface plasmon structure, Nat. Commun. **7**, 11619 (2016).

[18] L.-H. Wu and X. Hu, Scheme for Achieving a Topological Photonic Crystal by Using Dielectric Material, Phys. Rev. Lett. **114**, 223901 (2015).

[19] M. Z. Hasan and C. L. Kane, Colloquium: topological insulators, Rev. Mod. Phys. **82**, 3045 (2010); X.-L. Qi and S.-C. Zhang, Topological insulators and superconductors, Rev. Mod. Phys. **83**, 1057 (2011).

[20] T. Oka and H. Aoki, Photovoltaic Hall effect in graphene, Phys. Rev. B **79**, 081406(R) (2009).

[21] N. H. Lindner, G. Refael, and V. Galitski, Floquet topological insulator in semiconductor quantum wells, Nat. Phys. **7**, 490 (2011).

[22] Z. Gu, H. A. Fertig, D. P. Arovas, and A. Auerbach, Floquet Spectrum and Transport through an Irradiated Graphene Ribbon, Phys. Rev. Lett. **107**, 216601 (2011).

[23] J. Cayssol, B. Dóra, F. Simon, and R. Moessner, Floquet topological insulators, Phys. Status Solidi RRL **7**, 101 (2013).

[24] I. L. Garanovich, S. Longhi, A. A. Sukhorukov, and Yu. S. Kivshar, Light propagation and localization in modulated photonic lattices and waveguides, Phys. Rep. **518**, 1 (2012).

[25] M. Bukov, L. D'Alessio, and A. Polkovnikov, Universal high-frequency behavior of periodically driven systems: from dynamical stabilization to Floquet engineering, Adv. Phys. **64**, 139 (2015); R. Roy and F. Harper, Periodic table for Floquet topological insulators, arXiv:1603.06944.

[26] M. S. Rudner, N. H. Lindner, E. Berg, and M. Levin, Anomalous Edge States and the Bulk-Edge Correspondence for Periodically Driven Two-Dimensional Systems, Phys. Rev. X **3**, 031005 (2013).

[27] T. Kitagawa, E. Berg, M. Rudner, and E. Demler, Topological characterization of periodically driven quantum systems, Phys. Rev. B **82**, 235114 (2010).

[28] J. K. Asbóth, B. Tarasinski, and P. Delplace, Chiral symmetry and bulk-boundary correspondence in periodically driven one-dimensional systems, Phys. Rev. B **90**, 125143 (2014).

[29] P. Titum, N. H. Lindner, M. C. Rechstman, and G. Refael, Disorder-Induced Floquet Topological Insulators, Phys. Rev. Lett. **114**, 056801 (2015).

[30] D. Carpentier, P. Delplace, M. Fruchart, and K. Gawedzki, Topological Index for Periodically Driven Time-Reversal Invariant 2D Systems, Phys. Rev. Lett. **114**, 106806 (2015).
[31] P. Titum, E. Berg, M. S. Rudneer, G. Refael, and N. H. Lindner, The Anomalous Floquet-Anderson Insulator as a Nonadiabatic Quantized Charge Pump, Phys. Rev. X **6**, 021013 (2016).
[32] H. Wang, L. Zhou, and Y. D. Chong, Floquet Weyl phases in a three-dimensional network model, Phys. Rev. B **93**, 144114 (2016).
[33] Y. D. Chong and M. C. Rechtsman, Tachyonic dispersion in coherent networks, J. Opt. **18**, 014001 (2016).
[34] D. Marcuse, Radiation loss of a helically deformed optical fiber, J. Opt. Soc. Am. **66**, 1025 (1976).
[35] O. Peleg, G. Bartal, B. Freedman, O. Manela, M. Segev, and D. N. Christodoulides, Conical Diffraction and Gap Solitons in Honeycomb Lattices, Phys. Rev. Lett. **98**, 103901 (2007).
[36] Y. D. Chong, X.-G. Wen, and M. Soljačić, Effective theory of quadratic degeneracies, Phys. Rev. B **77**, 235125 (2008).
[37] X. Huang, Y. Lai, Z. H. Hang, H. Zhen, and C. T. Chan, Dirac cones induced by accidental degeneracy in photonic crystals and zero-refractive-index materials, Nat. Mater. **10**, 582 (2011).
[38] S.-L. Chua, L. Lu, J. Bravo-Abad, J. D. Joannopoulos, and M. Soljavić, Larger-area single-mode photonic crystal surface-emitting lasers enabled by an accidental Dirac point, Opt. Lett. **39**, 2072 (2014).
[39] F. D. M. Haldane, Model for a Quantum Hall Effect without Landau Levels: Condensed-Matter Realization of the, Parity Anomaly, Phys. Rev. Lett. **61**, 2015 (1988).
[40] L. Lu, C. Fang, L. Fu, S. G. Johnson, J. D. Joannopoulos, and M. Soljačić, Symmetry-protected topological photonic crystal in three dimensions, Nat. Phys. **12**, 337 (2016).
[41] H. Suzuura and T. Ando, Crossover from Symplectic to Orthogonal Class in a Two-Dimensional Honeycomb Lattice, Phys. Rev. Lett. **89**, 266603 (2002).
[42] G. Bergmann, Weak antilocalization—an experimental proof for the destructive interference of rotated spin 1/2, Solid State Commun. **42**, 815 (1982).
[43] T. Kitagawa, M. S. Rudner, E. Berg, and E. Demler, Exploring topological phases with quantum walks, Phys. Rev. A **82**, 033429 (2010); T. Kitagawa, M. A. Broome, A. Fedrizzi, M. S. Rudner, E. Berg, I. Kassal, A. Aspuru-Guzik, E. Demler, and A. G. White, Observation of topologically protected bound states in photonic quantum walks, Nat. Commun. **3**, 882 (2012).
[44] See Supplemental Material at http://link.aps.org/supplemental/10.1103/PhysRevLett.117.013902 for analysis of the tight binding model, detailed numerical methods, and further discussion of conical diffraction and disorder.
[45] A. Szameit and S. Nolte, Discrete optics in femtosecond-laser-written photonic structures, J. Phys. B **43**, 163001 (2010).
[46] T. Fukui, Y. Hatsugai, and H. Suzuki, Chern numbers in discretized Brillouin zone: efficient method of computing (spin) Hall conductances, J. Phys. Soc. Jpn. **74**, 1674 (2005).
[47] D. Song, V. Paltoglou, S. Liu, Y. Zhu, D. Gallardo, L. Tang, J. Xu, M. Ablowitz, N. K. Efremidis, and Z. Chen, Unveiling pseudospin and angular momentum in photonic graphene, Nat. Commun. **6**, 6272 (2015); F. Diebel, D. Leykam, S. Kroesen, C. Denz, and A. S. Desyatnikov, Conical Diffraction and Composite Lieb Bosons in Photonic Lattices, Phys. Rev. Lett. **116**, 183902 (2016).
[48] Y. Lumer, Y. Plotnik, M. C. Rechtsman, and M. Segev, Self-Localized States in Photonic Topological Insulators, Phys. Rev. Lett. **111**, 243905 (2013).